Romanian Reports in Physics, Vol. 65, No. 4, P. 1328–1347, 2013

A NOVEL SIMULATIONAL APPROACH: ELECTROMAGNETIC PARAMETERS DETERMINATIONS FOR SOME FERRITE-FERROELECTRIC NANOCOMPOSITES

D. IONESCU[1], G. APREOTESEI[2]

[1] "Gh. Asachi" Technical Univ. of Iasi, Department of Telecommunications, Carol I Blvd. 11, 700506 Iasi, Romania, E-mail: danaity@yahoo.com
[2] "Gh. Asachi" Technical Univ. of Iasi, Department of Physics, Dimitrie Mangeron Blvd. 67, 700050 Iasi, Romania, E-mail:gabiap03@yahoo.com

Received February 5, 2013

Abstract. A structural simulation strategy was developed for characterizing the ferromagnetic-ferroelectric systems (hexagonal ferrite-ferroelectric perovskite) which were synthesized like high permeability and high permittivity nanocomposites. These quantities were determined in the NATO K band (20 to 40 GHz) and their evolutions with different parameters were linked on the intrinsic characteristics of constituent phases. A derived mixture law with coefficients depending on relative volume fractions, substitution ion radii, hexaferrite internal order (M or Y type), respectively the polarizing fields was synthesized. A ferromagnetic-ferroelectric system tunability ranging from 4 to 28% was achieved, depending upon each structure characteristics.

Key words: nanocomposite, hexagonal ferrite, ferroelectric perovskite, effective permittivity, permeability, derived mixture law, tunability.

1. INTRODUCTION

The ferrite-ferroelectric nanocomposites are of special interest for their both high electric permittivity and high magnetic permeability. Combinations of this type are the hexagonal ferrite-ferroelectric perovskite, with different relative volume fractions. The system will be denoted: (1–*y*) ferrite / (*y)* ferroelectric phase. The *M* type, respectively *Y*-type hexaferrite were considered for our study, associated usually with perovskites like barium strontium titanate BSTO or PNNT ceramics.

In the ferrite-ferroelectric composite ceramics, the spinel ferrites like NiCuZn ferrite are used as magnetic phase, for their compatibility with the LTCC manufacturing process. For higher frequency applications, the hexagonal ferrites are recommended, such as the barium ferrites: *M* type ($Ba_{1-a}Me_aFe_{12}O_{19}$), *Y*-type

($Ba_2Me_2Fe_{12}O_{22}$) or *Z*-type ($Ba_3Me_2Fe_{24}O_{41}$), where *Me* is a divalent transition metal or a group of two divalent metals in a proper volume ratio.

A high crystallographic anisotropy characterizes the ferrites. All their behavior is dominated by the consequences of the high anisotropy existence. In the case of spinels the internal anisotropy field is three orders lower than that of hexagonal ferrites, determining the placement of the domain for the ferromagnetic resonance at frequencies lower than a few hundred of MHz. The ferromagnetic resonance occurs in hexagonal ferrites above a few GHz, up to 200 GHz, which make then very attractive for microwave applications. The corresponding anisotropy field is of tens of Oersted to dozens of kilooersted and no polarizing field is required for the material to exhibit an important magnetization. The advantages of tunability of the magnetic anisotropy and low microwave losses are to be mentioned.

The hexaferrites present also an excellent sintering behavior in association with the BSTO ferroelectrics.

2. SIMULATION MODEL OF THE FERRITE-FERROELECTRIC MEDIUM

The nanocomposites of hexagonal ferrite-ferroelectric perovskite considered for our study consist of the magnetic phase and the ferroelectric phase, which have specific characteristics.

The magnetic phase is represented of a *M* or *Y* type hexaferrite, having the basic electromagnetic parameters as follows:

– *M* type, *Me*-M: $Ba_{1-a}Sr_aFe_{12}O_{19}$ (BSFO, a = 0–1). An effective magnetic permeability μ_{eff} of circa 36.3 characterizes the polycrystalline barium strontium hexaferrite (BSFO) and an effective electric permittivity ε_{eff} of circa 8.18 at 1 GHz [1, 2]. Both electromagnetic parameters depend on substitution degree of the Ba ions with Sr and decrease with a few percents in microwave range. Grain sizes of 40–100 nm are typical for the polycrystalline pure phase.

– *Y* type, Me_2Y: $Ba_2Zn_2Fe_{12}O_{22}$ (Zn_2Y), respectively $Ba_2Zn_{2-c}Cu_cFe_{12}O_{22}$ (BZCF, c = 0–0.8). The Zn_2Y has a μ_{eff} of 24 and an ε_{eff} of 16.2 at 1 GHz [2], with a slow variation with frequency. Grain sizes are of 0.8 - 4.7 μm. The Cu-modified Zn_2Y ferrite, also called BZCF, presents similar parameters: a μ_{eff} of 26.7 and an ε_{eff} of 19.3 at 1 GHz [2, 3], presenting a variation in function of the substitution degree and of the substituent type. The grain sizes of BZCF are of 0.8–3.6 μm.

The magnetic permeability of the magnetic phase can be modified considering that the magnetism of polycrystalline ferrites is a consequence of spin rotation and domain walls motion. The control parameters are: the grain size, densification, an applied static field *H*, internal stress, etc.

The ferroelectric phase in the nanocomposite is represented by a ferroelectric perovskite:

– $Ba_xSr_{1-x}TiO_3$ (BSTO, x = 0.75–1). The BSTO presents an effective permittivity of 2620–3740 at 1 GHz [4, 5], which is function on substituting ions content in the perovskite for a constant bias voltage of 12 kV/cm and does not exhibit a significant frequency dependence in microwave range. The average grain size is of 18–48 nm in the pure phase. The tunability of the permittivity can be achieved by changing the bias field, usually in the range of 2–20 kV/cm and also considering the modifications in microstructure including the grain size, interfacial amorphous layer, texture misalignment, surface roughness and deterioration of the Bragg reflector layers [6].

The values for the electromagnetic parameters for the pure phases were obtained with a fair enough precision (less than 2% relative error) with our simulation method using the HFSS program, based on the material models included in our data base [7, 8].

The simulation model for the ferromagnetic-ferroelectric systems was developed on the basis of the structure details for each phase and considering the internal interactions between the components and the interaction with the applied fields.

The $Ba_{1-a}Sr_aFe_{12}O_{19}$ M type hexaferrite is characterized by a RSR*S* crystallographic build up, with 2M number of molecules per unit cell, space group $P6_3/mmc$ (Fig. 1a). The structure is hexagonal, represented by a backbone of oxygen anions, the interstices of the close-packed oxygen lattice being occupied by metallic cations, magnetic and nonmagnetic. The cations usually have either four- or six-fold coordination and form tetrahedral, octahedral or trigonal sublattices. The hexaferrite presents high uniaxial anisotropy, with c-axis (easy magnetization axis) of 23.2 Å (Fig. 1b). Magnetic properties arise from the super-exchange mechanism [9, 10, 16]. The cation spins are antialigned and the total magnetization can be increased by creating an imbalance between the sublattice magnetizations using substitution cations. The substitution cation must be carefully chosen to maximize magnetization and maintain a strong exchange constant. The magnetic moment is high – the pure strontium hexaferrite has the total magnetic moment of 20 μ_B. The saturation magnetization depends on the distribution of the substituted ions at different sites in the crystal structure and the electronic configuration. The hexaferrite system is a dielectric material, with a good thermal and chemical stability.

The Y type hexaferrites have a rhombohedral structure, with crystallographic build up 3TS and a 3MeY number of molecules per unit cell, space group R-3/m. The crystalline structure is built up as a superposition of S and T blocks (Fig. 2a). The unit cell is composed of the sequence STSTST including three formula units (Fig. 2b). The metallic cations are distributed among six sublattices with different number of ions, which impose the spin configuration of the ferrite. The haxaferrite has planar anisotropy, with a c-axis (hard axis) of 43.56 Å.

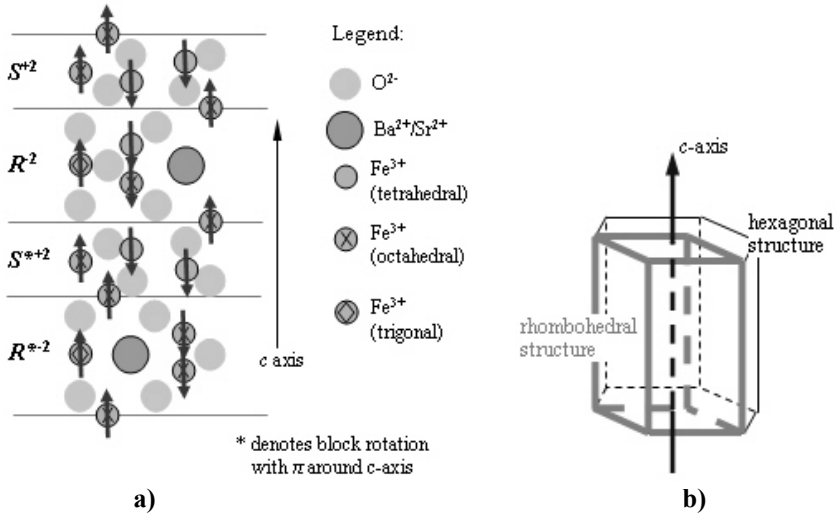

Fig. 1 – a) The RSR*S* block structure of the Ba-M hexaferrite, with the spin configuration. The easy magnetization direction is along the crystallographic *c*-axis; b) hexagonal / rhombohedral structure with the *c* magnetization axis.

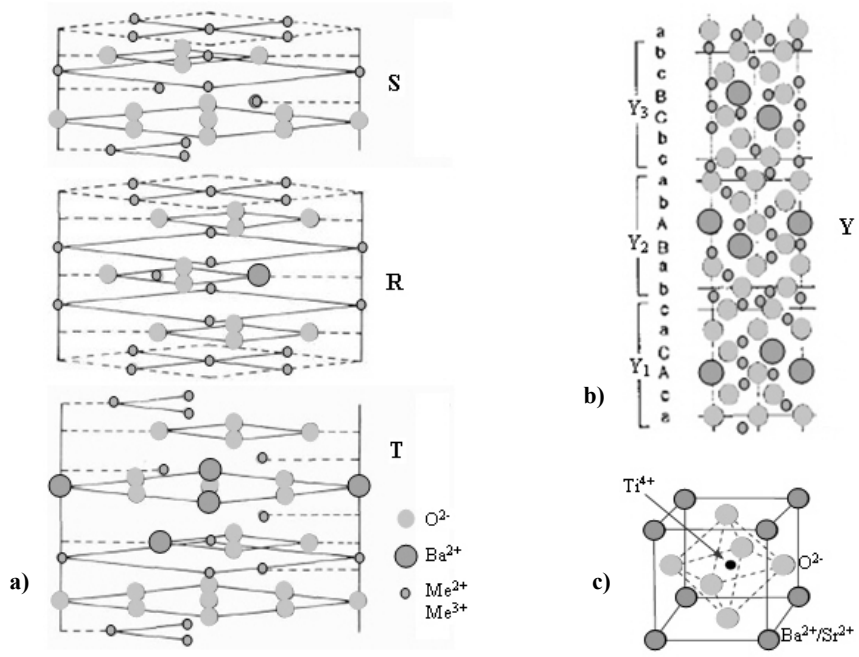

Fig. 2 – a) The S, R, T structural blocks included in the hexaferrites. Blocks can be rotated in a succession specific to each configuration (*M*,*Y*,*Z*); b) the crystallographic build up of the *Y* type hexaferrites; a, b, c – close-packed oxigen layers; A, B, C – mixed Ba-O layers (after van Landuyt *et al.*, 1974); c) the perovskite structure of the ferroelectric phase, $Ba_xSr_{1-x}TiO_3$.

For a single crystal of hexaferrite, the ferromagnetic resonant frequency can be estimated with Kittel's formula:

$$f_0 \cong \gamma_1 \sqrt{(H + H_a) \cdot (H + H_a + 4\pi M_S)}, \quad (1)$$

where $4\pi M_s$ is the saturation magnetization (*e.g.* 4.8 kG for Ba-*M*, 2.85 kG for Zn_2Y); H_a is the anisotropy field (*e.g.* 19 kOe for Ba-*M*, -9 kOe for Zn_2Y), depending on the hexaferrite and the gyromagnetic ratio $\gamma_1 = \left|\vec{\mu}_B\right| / \left|\vec{s}\right|$ = 2.8 GHz·kOe^{-1} [1]. The external bias magnetic field was taken in range of 5 ÷ 10 kOe.

The electric permittivity usually lower than 20, which characterizes the barium hexaferrites, is obtained by simulation if we consider the dielectric mechanism of ferrite which is associated with the conduction mechanism, attributed to the easy electron transfer between Fe^{2+} and Fe^{3+} ions.

The $Ba_xSr_{1-x}TiO_3$ is derived from the $BaTiO_3$ tetragonal ferroelectric perovskite by partial substituting of the barium ions with strontium. The crystal structure is tetrahedral (Fig. 2c), space group *P4mm* (lattice parameters: a = 3.992 Å, c = 4.036 Å). The [001] is the polar axis and material presents a spontaneous polarization P_S of around 0.22 C/m^2 at room temperature. The grain sizes in the polycrystalline phase are of a few hundreds of nm, with polyhedron particle shapes. The perovskite does not have magnetic properties (μ_r =1).

The substitution degree is important for the $Ba_xSr_{1-x}TiO_3$ compound: for x = 0.75 ÷ 1 the material is a ferroelectric tetragonal perovskite, otherwise it becomes a paraelectric cubic perovskite and it is no more of interest for the synthesis of a ferrite-ferroelectric nanocomposite.

The combinations of the considered magnetic and ferroelectric phases were:

– (1–y) $Ba_{1-a}Sr_aFe_{12}O_{19}$ / y $Ba_xSr_{1-x}TiO_3$, with y = 0.5 ÷ 0.9; a = 0 ÷ 1; x = 0.75 ÷ 1

– (1–y) $Ba_2Zn_{2-c}Cu_cFe_{12}O_{22}$ / y $Ba_xSr_{1-x}TiO_3$, with y = 0.3÷ 0.9; c = 0–0.8; x = 0.75 ÷ 1.

These nanocomposites are prepared in practice by sintering at 1200–1220 ^{0}C for circa 3 h after mixing and milling for 2 h [1, 11, 12]. The mixture is obtained by ions diffusion between the ferrite and ferroelectric grains during the sintering process at high temperature [13, 14, 15]. The microstructure and properties of the composite depend on the thickness of diffusion layer and element distribution in this layer and can be reproduced by simulation. The diffusion coefficient is function of the ion's radius and charge, indicated in Table 1.

The average size of ferrite / ferroelectric grains decreases with the rise of corresponding phase concentration in the mixture. The ferrite grains have sizes of circa 200 ÷ 300 nm, the ferroelectric grains being smaller, with sizes less than 200 nm [14]. Magnetoelectric interactions occur between ferroelectric and ferromagnetic grains, determining the agglomeration of ferrite grains with ferroelectric grains.

Table 1

Ionic radius of different atomic species included in the ferrite-ferroelectric nanocomposite

Ion	Ba^{2+}	Ti^{4+}	Fe^{3+}	Fe^{2+}	Co^{2+}	Zn^{2+}
Ionic radius [nm]	0.135	0.074	0.076	0.064	0.074	0.074
Magnetic moment ($\mu_{spin\text{-}only}/\mu_B$)	0	0	5.92	4.90	3.88	0
Ion	Cu^{2+}	Mn^{3+}	Mg^{2+}	Sr^{2+}	O^{2-}	
Ionic radius [nm]	0.072	0.066	0.086	0.158	0.126	
Magnetic moment ($\mu_{spin\text{-}only}/\mu_B$)	1.73	4.90	0	0	0	

3. PHYSICAL ALGORITHM FOR ELECTROMAGNETIC PARAMETERS DETERMINATION

The perovskite-type material with crystalline nanograins is non-linear and electric anisotropic. Polarization and electric displacements as responses of the material at the excitation field are non-linear and can be written as [1, 5]:

$$\boldsymbol{P} = \chi_e^{(1)}\boldsymbol{E} + \chi_e^{(2)}\boldsymbol{E}^{2+} + ... = \overline{\overline{\chi_e}}(\boldsymbol{E})\cdot\boldsymbol{E}\,, \tag{2}$$

$$\boldsymbol{D} = \varepsilon_0\boldsymbol{E} + \boldsymbol{P} = \varepsilon_0\overline{\overline{\varepsilon_r}}\boldsymbol{E}\,. \tag{3}$$

In the same time, for the ferrite, which is a non-linear material, one can write:

$$\boldsymbol{B} = \mu_0\left(\boldsymbol{H} + \boldsymbol{M}\right) = \mu_0\overline{\overline{\mu_r}}\boldsymbol{H}\,, \tag{4}$$

$$\overline{\overline{\mu}} = \mu_0\left(1 + \overline{\overline{\chi_m}}\right); \qquad \overline{\overline{\chi_m}} = \begin{vmatrix} \chi_m & j\kappa & 0 \\ j\kappa & \chi_m & 0 \\ 0 & 0 & 0 \end{vmatrix}, \tag{5}$$

where $\boldsymbol{E}$ = electric intensity vector; $\boldsymbol{D}$ = electric displacement vector; $\boldsymbol{P}$ = polarization vector; $\overline{\overline{\chi_e}}$ = electric susceptibility tensor; $\overline{\overline{\varepsilon_r}}$ = electric relative permittivity tensor; ε_0, μ_0 = electric permittivity / magnetic permeability of vacuum; $\boldsymbol{H}$ = magnetic intensity vector; $\boldsymbol{B}$ = magnetic induction vector; $\boldsymbol{M}$ = magnetization vector; $\overline{\overline{\chi_m}}$ = magnetic susceptibility tensor; $\overline{\overline{\mu_r}}$ = magnetic relative permeability tensor.

The $\overline{\overline{\chi_e}}(\boldsymbol{E})$ / $\overline{\overline{\chi_m}}$ functions depend on crystalline phase structure and the structure of nonograins. The parametric susceptibilities $\overline{\overline{\chi_e}}(\boldsymbol{E})$ / $\overline{\overline{\chi_m}}$ can be determined with help of the simulation program by reporting the emergent to incident field parameters [8, 17].

The physical algorithm for determination of the electromagnetic parameters of the nanocomposite is based on the calculation of the energy density variation when the testing field propagates through the material sample. We have used the Poynting's theorem in integral form [1]:

$$\frac{\partial}{\partial t} w \cdot dV + \oint_{\partial V} \boldsymbol{S}_{Poynting} \cdot d\boldsymbol{A} = -\int_V \boldsymbol{J} \cdot \boldsymbol{E} \cdot dV \,, \tag{6}$$

where $S_{Poynting}$ is the Poynting vector, $\boldsymbol{S}_{Poynting} = \boldsymbol{E} \times \boldsymbol{H}$ represents the energy density, $w = w_e + w_m$; $\boldsymbol{J}$ is the current density and ∂V is the surface which encloses the sample volume V.

For a finite number of the sinusoidal field periods, the dw_e, respectively dw_m variations are linked by the electric susceptibility $\overline{\overline{\chi_e}}(\boldsymbol{E})$, respectively by the magnetic susceptibility $\overline{\overline{\chi_m}}$ tensor components:

$$dw_e = \boldsymbol{E} \cdot d\boldsymbol{P} = \boldsymbol{E} \cdot d\left(\varepsilon_0 \cdot \overline{\overline{\chi_e}} \cdot \boldsymbol{E} \right) = \varepsilon_0 \cdot \left(\boldsymbol{E} \cdot \overline{\overline{\chi_e}} \cdot d\boldsymbol{E} \right), \tag{7}$$

$$dw_m = \boldsymbol{H} \cdot d\boldsymbol{M} = \boldsymbol{H} \cdot d\left(\overline{\overline{\chi_m}} \cdot \boldsymbol{H} \right) = \left(\boldsymbol{H} \cdot \overline{\overline{\chi_m}} \cdot d\boldsymbol{H} \right). \tag{8}$$

For the susceptibility determinations, the dw_e, respectively dw_m variations were calculated using the data given by the HFSS program. By varying the excitation field frequency, the parametrical evolutions of the nanocomposite permittivity and permeability were obtained, in the considered frequency range (20 -40 GHz).

4. RESULTS FOR THE ELECTROMAGNETIC PARAMETERS

Electric permittivity and magnetic permeability values were calculated for the considered ferrite-ferroelectric nanocomposites. The polarizing field levels were of 5–10 kOe (5 kOe as reference) for the external magnetic field $\boldsymbol{H}$ and of 2–20 kV/cm (12 kV/cm as reference) for the electric field $\boldsymbol{E}$. Results were obtained for the frequency range of 20 to 40 GHz. Simulations were performed at room temperature.

Evolutions of the nanocomposite electromagnetic parameters were represented on surface plots: the effective permittivity in function of the concentration and permittivity of the ferroelectric phase, respectively the effective permeability in function of the concentration and permeability of the ferrite. In Figs. 3, 4 are given the results for the composite with *M* type hexaferrites. In Figs. 5, 6 are represented the plots corresponding to the composite with *Y* type hexaferrites. Thus, on each plot, around the red curves, one can find the results correspond to the following

composites analyzed here (the whole plots were drawn for a large range of permittivities / permeabilities for the constituent phases):

– for ε_{eff} plots:

(1–*y*) $Ba_{0.8}Sr_{0.2}Fe_{12}O_{19}$ / *y* $Ba_xSr_{1-x}TiO_3$ with $y = 0.5 \div 0.9$; $x = 0.75 \div 1$ – in Fig. 3

(1–*y*) $Ba_2Zn_2Fe_{12}O_{22}$ / *y* $Ba_xSr_{1-x}TiO_3$ with $y = 0.3 \div 0.9$; $x = 0.75 \div 1$ – in Fig. 4;

– for μ_{eff} plots:

(1–*y*) $Ba_{1-a}Sr_aFe_{12}O_{19}$ / *y* $Ba_{0.9}Sr_{0.1}TiO_3$ with $y = 0.5 \div 0.9$; $a = 0 \div 1$ – in Fig. 5

(1–*y*) $Ba_2Zn_{2-c}Cu_cFe_{12}O_{22}$ / *y* $Ba_{0.9}Sr_{0.1}TiO_3$ with $y = 0.3 \div 0.9$; $c = 0$–0.8 – in Fig. 6.

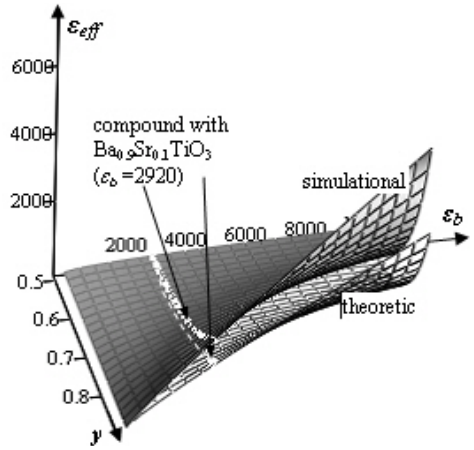

Fig. 3 – Effective permittivity evolution *versus* ferroelectric phase permittivity and concentration, for the nanocomposite with *M* type hexaferrite ($\varepsilon_{a,M} = 8.18$ = ct. for $Ba_{0.8}Sr_{0.2}Fe_{12}O_{19}$).

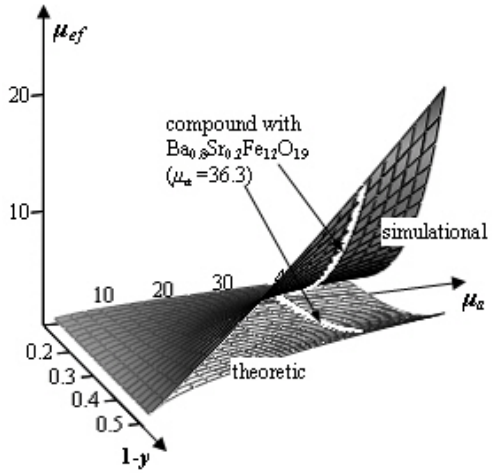

Fig. 4 – Effective permeability evolution *versus* ferrite phase permeability and concentration, for the nanocomposite with *M* type hexaferrite; the perovskite ($Ba_{0.9}Sr_{0.1}TiO_3$) has no magnetic properties ($\mu_b = 1$ = ct.).

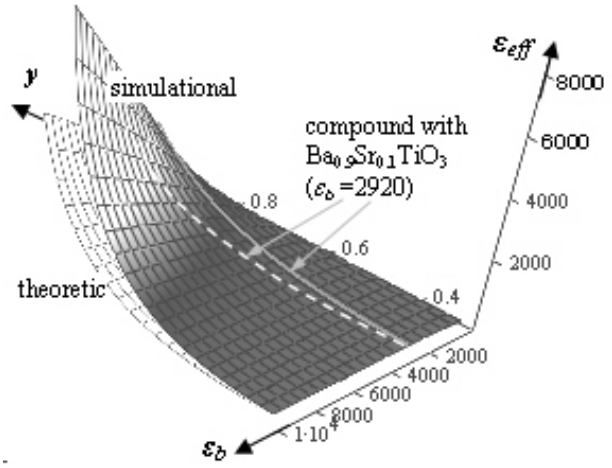

Fig. 5 – Effective permittivity evolution *versus* ferroelectric phase permittivity and concentration, for the nanocomposite with *Y* type hexaferrite ($\varepsilon_{a,Y}$ = 16.2 = ct. for $Ba_2Zn_2Fe_{12}O_{22}$).

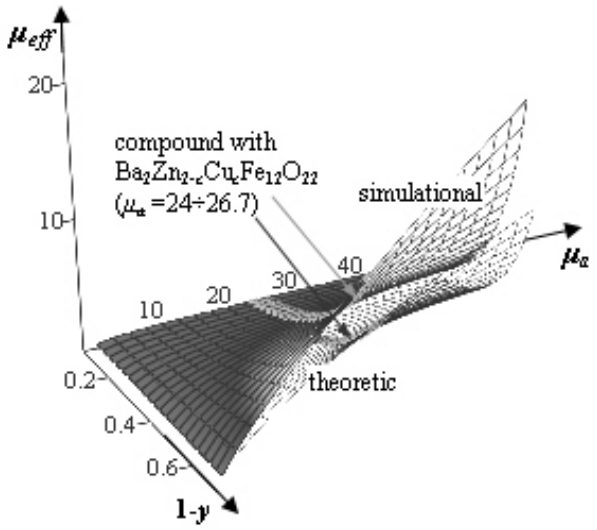

Fig. 6 – Effective permeability evolution *versus* ferrite phase permeability and concentration, for the nanocomposite with *Y* type hexaferrite; the perovskite ($Ba_{0.9}Sr_{0.1}TiO_3$) has no magnetic properties (μ_b = 1 = ct.).

Graphs are presenting the simulational, respectively theoretical surface plots for the effective permittivity / permeability of the composites. The theoretical plots were represented using the mixture law [1], written for a composite material with powder mixture:

$$\ln \psi^* = f_a \cdot \ln \psi_a + f_b \cdot \ln \psi_b , \tag{9}$$

where f_a, respectively f_b represent the volume fractions of each phase; ψ^* is the effective value of the electric permittivity or magnetic permeability of the composite; ψ_a, respectively ψ_b are the permittivity or permeability for each phase: *a* – ferrite, *b* – ferroelectric. If the ferroelectric phase concentration is denoted with *y*, the relation (9) can be written:

$$\ln \varepsilon_{eff} = (1-y) \cdot \ln \varepsilon_a + y \cdot \ln \varepsilon_b , \tag{10}$$

$$\ln \mu_{eff} = (1-y) \cdot \ln \mu_a + y \cdot \ln \mu_b . \tag{11}$$

Electromagnetic properties of the ferrite-ferroelectric nanocomposites are determined by the concentration of phases and their internal properties.

Graphs for the effective permittivity indicate us that higher values can be obtained rather by the ferroelectric phase concentration increasing than by using ferroelectrics with high permittivity. For ferroelectrics with permittivity higher than 6 000, the nanocomposite permittivity increases abruptly indeed, but such ferroelectrics are more difficult to be obtained and controlled inside the composite at field application. The ferroelectric ceramics are proper materials for such nanocomposites, having significant permittivity (higher than several thousands) owing to the polarization of dipolar and presenting a high chemical stability. The simulation results have also illustrated low dielectric losses for the analyzed nanocomposites.

The simulational (colormap) surfaces are situated above the theoretic (wireframe) plots, illustrating a more dynamic evolution of the effective parameters with respect to the phase concentration and component parameters than the theory predicts. The curves corresponding to the particular value of the ferroelectric permittivity (ε_b = 2 920 for $Ba_{0.9}Sr_{0.1}TiO_3$) were represented on graphs with the red lines, for comparison. Different coefficients characterize the mathematical description of the plots, corresponding to the two different types of hexaferrites included in the nanocomposite. Coefficients dependence on the internal parameters and polarizing fields will be illustrated in the followings.

Simulational graphs for the effective permeability of the composite separate consistently from the theoretical plots when the permeability of the ferrite phase increases, more accentuated for the compounds with *M* type hexaferrite. Internal properties of the ferrite phase influence the plots shape, the structure with high uniaxial anisotropy (*M* type) determining a nanocomposite with μ_{eff} increasing more abruptly with ferrite permeability, than the structure with planar anisotropy (*Y* type). The red curves corresponding to particular compounds mentioned above illustrate this evolution.

We have also to observe that the effective permeability of the compound decrease rapidly with increasing the BSTO content (the ferroelectric phase). A nanocomposite with at least 40 % ferrite phase presents an effective permeability comparable with at least half of ferrite permeability and the μ_{eff} values are good controllable with help of different internal or external parameters.

A derived mixture law can be formulated on the basis of simulational 3D plots, with coefficients depending on different factors like: substitution degree in the compound constituents, substitution ions radius and charge, substitution ions magnetic moment, ferrite internal order, polarizing fields. The mathematical description of the effective permittivity, respectively permeability of the ferrite - ferroelectric nanocomposite is given by:

$$ct \cdot \left(\ln \varepsilon_{eff}\right)^{ct'} = ct_a \cdot (1-y) \cdot \left(\ln \varepsilon_a\right)^{ct_a'} + y \cdot \left(\ln \varepsilon_b\right)^{ct_b'} \tag{12}$$

$$cs \cdot \left(\ln \mu_{eff}\right)^{cs'} = (1-y) \cdot \left(\ln \mu_a\right)^{cs_a'} + cs_b \cdot y \cdot \left(\ln \mu_b\right)^{cs_b'} \tag{13}$$

A set of values for the coefficients in relations (12), (13) is indicated in Table 2, as example. The *M* ferrite combination, respectively the *Y* ferrite combination for which these coefficients are valuable were:

– (1–*y*) $Ba_{0.8}Sr_{0.2}Fe_{12}O_{19}$ / *y* $Ba_{0.9}Sr_{0.1}TiO_3$ with ($y = 0.5 \div 0.9$)

– (1–*y*) $Ba_2Zn_{2-c}Cu_cFe_{12}O_{22}$ / *y* $Ba_{0.9}Sr_{0.1}TiO_3$ with ($y = 0.3 \div 0.9$; $c = 0.8$).

Table 2

Coefficients of the derived mixture law for the ferrite-ferroelectric nanocomposite with two different types of hexaferrite (*M* and *Y* type): (1–*y*) $Ba_{0.8}Sr_{0.2}Fe_{12}O_{19}$ / *y* $Ba_{0.9}Sr_{0.1}TiO_3$, $y = 0.5 \div 0.9$, respectively (1–*y*) $Ba_2Zn_{1.2}Cu_{0.8}Fe_{12}O_{22}$ / *y* $Ba_{0.9}Sr_{0.1}TiO_3$, $y = 0.3 \div 0.9$.

	ct	ct'	ct_a	ct_a'	ct_b'	cs	cs'	cs_a'	cs_b	cs_b'
M ferrite combination	0.874	1.424	0.983	1.046	1.385	0.972	1.116	1.458	0.847	1.025
Y ferrite combination	0.893	1.415	0.972	1.035	1.396	0.924	1.213	1.226	0.928	1.015

Coefficients of the derived mixture law evolve with respect to different parameters in a manner presented in Figs. 7–9 and Tables 3, 4.

The dependence on the internal parameters of the ferroelectric phase properties can be illustrated by representing the coefficients modification with respect to the substitution degree of the Ba ions with Sr in the barium perovskite lattice, *x* (Fig. 7). The illustrated results correspond to the composites:

– (1–y) $Ba_{0.8}Sr_{0.2}Fe_{12}O_{19}$ / y $Ba_xSr_{1-x}TiO_3$ (y = 0.5 ÷ 0.9, with x varying from 0.75 to 1)

– (1-y) $Ba_2Zn_{1.2}Cu_{0.8}Fe_{12}O_{22}$ / y $Ba_xSr_{1-x}TiO_3$ (y = 0.3÷ 0.9, with x varying from 0.75 to 1).

The coefficients in relation (12) which describe the effective permittivity of the nanocomposite are decreasing with x, while the effective permeability of the nanocomposite is practically not influenced (coefficients in relation (13) are about the same).

The coefficients determined for a group of values for x are given also in Table 3. Substitution degree variation determines a modification of the ferroelectric phase permittivity and consequently a modification of the effective permittivity of the nanocomposite. Derived mixture law coefficient modifications are linked by the physical mechanism of permittivity modification by partial substitution of ions species in the ferroelectric material.

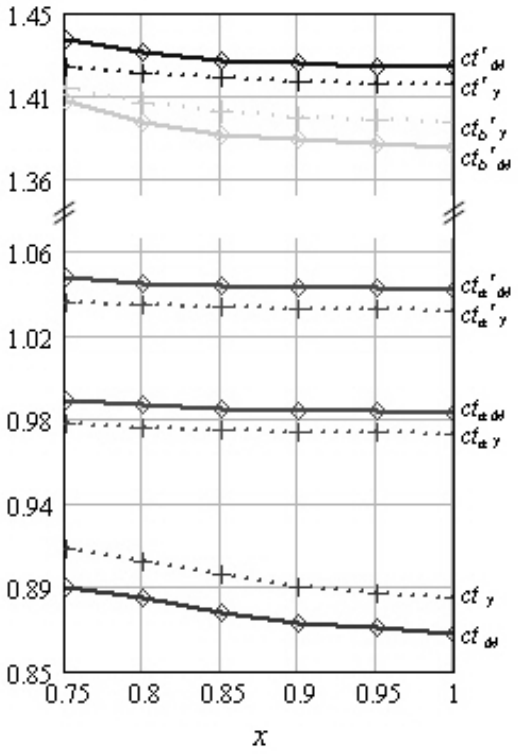

Fig. 7 – Evolution of the derived mixture law coefficients for effective permittivity of the nanocomposite versus the substitution degree in the ferroelectric phase. Coefficients are given for the combinations with *M*, respectively *Y* hexaferrite.

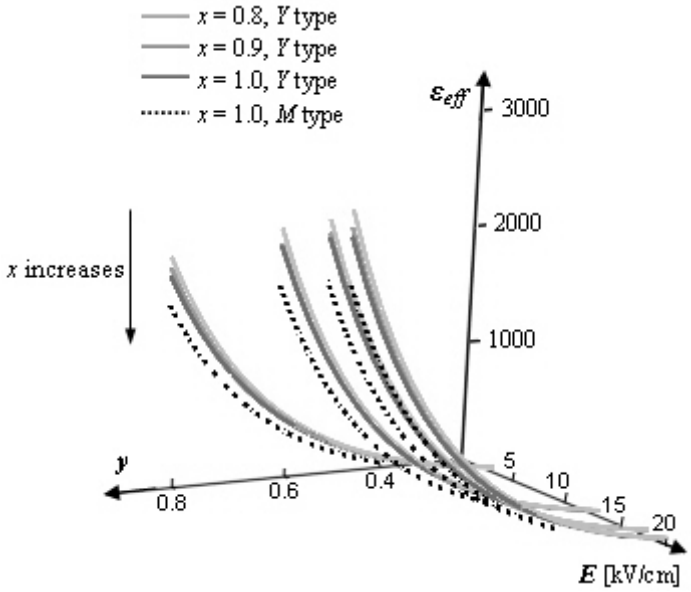

Fig. 8 – Effective permittivity *versus* ferroelectric phase concentration, for different values of the polarizing field *E*, in the case of the nanocomposites with *Y* type hexaferrite: (1–*y*) $Ba_2Zn_{1.2}Cu_{0.8}Fe_{12}O_{22}$ / *y* $Ba_xSr_{1-x}TiO_3$ having different *x*. Minimal dotted curves are given for the compound with *M* hexaferrite: ($Ba_{0.8}Sr_{0.2}Fe_{12}O_{19}$) / *y* $Ba_xSr_{1-x}TiO_3$, with $x = 1$.

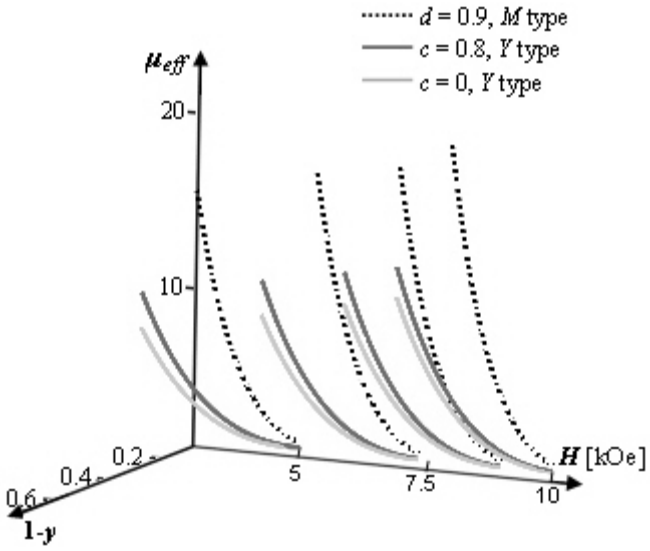

Fig. 9 – Effective permeability *versus* ferrite phase concentration, for different values of the polarizing magnetic field *H*, in the case of the nanocomposite with *Y* hexaferrite: (1–*y*) $Ba_2Zn_{2-c}Cu_cFe_{12}O_{22}$ / *y* $Ba_{0.9}Sr_{0.1}TiO_3$ having different *c*, respectively with *M* hexaferrite: (1–*y*) $Ba_{0.8}Sr_{0.2}Co_{2d}Fe_{(12-2d)}O_{19}$ / *y* $Ba_{0.9}Sr_{0.1}TiO_3$, with $d = 0.9$.

Table 3

Values of the coefficients in the derived mixture law for permittivity, using different substitution degrees, x, in the barium perovskite

	x	ct	ct'	ct_a	ct_a'	ct_b'
M ferrite combination $(1-y)Ba_{0.8}Sr_{0.2}Fe_{12}O_{19}$ / y $Ba_xSr_{1-x}TiO_3$	0.75	0.893	1.436	0.989	1.052	1.405
	0.80	0.887	1.430	0.986	1.048	1.394
	0.85	0.880	1.426	0.984	1.047	1.387
	0.90	0.874	1.424	0.983	1.046	1.385
	1.00	0.872	1.422	0.983	1.046	1.383
Y ferrite combination $(1-y)Ba_2Zn_{1.2}Cu_{0.8}Fe_{12}O_{22}$ / y $Ba_xSr_{1-x}TiO_3$	0.75	0.913	1.422	0.977	1.039	1.411
	0.80	0.906	1.419	0.975	1.037	1.404
	0.85	0.899	1.417	0.973	1.036	1.399
	0.90	0.893	1.415	0.972	1.035	1.396
	1.00	0.890	1.414	0.972	1.035	1.395

Values obtained for the nanocomposite effective permittivity are punctually confirmed by experimental results found in literature, in the considered frequency range ([9, 2] and so on). The medium relative error was less or equal than 4 %, for the whole considered domain of variation for x.

Table 4

Values of the coefficients in derived mixture law for permeability, obtained for different substitution ions in hexaferrite

***M* ferrite combination**: $(1-y)$ $\mathbf{Ba_{(1-a)}Me^{2+}_aMe1^{3+}_{2d}Fe_{(12-2d)}O_{19}}$ / y $Ba_{0.9}Sr_{0.1}TiO_3$								
Substitution ion (1) / Substituted ion (2)	Substitution degree	r [nm] (1) / r [nm] (2)	$\mu_{spin\text{-}only}/\mu_B$ (1) / $\mu_{spin\text{-}only}/\mu_B$ (2)	cs	cs'	cs_a'	cs_b	cs_b'
Sr^{2+}/Ba^{2+}	a = 0.9	0.158 / 0.135	0 / 0	0.973	1.116	1.456	0.847	1.025
Co^{2+}/Fe^{3+}	d = 0.9	0.074 / 0.076	3.88 / 5.92	0.976	1.115	1.442	0.848	1.025
Zr^{4+}/Fe^{3+}	d = 0.9	0.086 / 0.076	0 / 5.92	0.980	1.112	1.422	0.849	1.024
Sc^{3+}/Fe^{3+}	d = 0.9	0.088 / 0.076	0 / 5.92	0.981	1.112	1.420	0.849	1.024
***Y* ferrite combination**: $(1-y)$ $\mathbf{Ba_{(2-e)}Me1^{2+}_eZn^{2+}_{(2-e)}Me2^{2+}_eFe_{12}O_{22}}$ / y $Ba_{0.9}Sr_{0.1}TiO_3$								
Substitution ion (1) / Substituted ion (2)	Substitution degree	r [nm] (1) / r [nm] (2)	$\mu_{spin\text{-}only}/\mu_B$ (1) / $\mu_{spin\text{-}only}/\mu_B$ (2)	cs	cs'	cs_a'	cs_b	cs_b'

Table 4 (continued)

Sr^{2+}/Ba^{2+}	$e = 1.8$	0.158 / 0.135	0 / 0	0.927	1.211	1.214	0.929	1.015
Cu^{2+}/Zn^{2+}	$c = 0.8$	0.072 / 0.074	1.73 / 0	0.924	1.213	1.226	0.928	1.015
Co^{2+}/Zn^{2+}	$c = 0.9$	0.074 / 0.074	3.88 / 0	0.921	1.215	1.237	0.927	1.016
Mg^{2+}/Zn^{2+}	$c = 2.0$	0.086 / 0.074	0 / 0	0.929	1.211	1.217	0.929	1.015
Mn^{2+}/Zn^{2+}	$c = 1.0$	0.066 / 0.074	4.90 / 0	0.919	1.214	1.246	0.926	1.016

Magnetic properties and dimensions of the substitution ions influence the effective permeability of the nanocomposite due to the fact that ions with different size and magnetic moment are modifying the spin equilibrium configuration of the hexaferrite. The coefficient values of the derived mixture law for the effective permeability of the nanocomposite are indicated in Table 4, for different substitution ions in the ferrite phase. Substitution degree was chosen equal or close to the maximum value for which the material properties are convenient (material has great and controllable magnetic permeability). The illustrated results correspond to the composites:

– $(1–y)\ Ba_{(1-a)}Me^{2+}_{a}Me1^{3+}_{2d}Fe_{(12-2d)}O_{19} / y\ Ba_{0.9}Sr_{0.1}TiO_3$ (with different a, d);

– $(1–y)\ Ba_{(2-e)}Me1^{2+}_{e}Zn^{2+}_{(2-c)}Me2^{2+}_{c}Fe_{12}O_{22} / y\ Ba_{0.9}Sr_{0.1}TiO_3$ (with different e, c).

In the *M* type hexaferrite, by substituting the Ba ions without magnetic moment with ions also without magnetic moment, the effective permeability of the nanocomposite decreases insignificantly, due to a slight modification of the equilibrium configuration by the Sr ions with bigger radius. The Co ions substituting the Fe ions with higher magnetic moment determine a decreasing of the effective permeability [18], illustrated in our case by the evolution of the derived mixture law coefficients. Effective permeability decreasing by substituting the Fe ions with ions without magnetic moment is more accentuated.

For the *Y* type hexaferrite, by substituting the Zn ions without magnetic moment with Cu ions with a low magnetic moment, an effective permeability increasing occurs. Substitution with ions having higher magnetic moment (Co, Mn) determine also the composite permeability increasing, while for substituting ions without magnetic moment the permeability variation is very low, the ions radii ratio being important in this case. (Effective permeability evolves in the same manner like the cs_a' coefficient of the magnetic phase, in Table 4.)

The continuous polarizing fields (***E***, ***H***) were varied for estimating their influence on the electromagnetic parameters of the ferrite-ferroelectric nanocomposite. The dependence of the *S*-parameters on the applied fields determines a variation of the effective permittivity / permeability of the nanocomposite, illustrated by the simulational 3D plots in Figs. 8–9. The polarizing

field variation range was of 5-10 kOe for the external magnetic field ***H*** and of 2–20 kV/cm for the electric field ***E***.

The ferrite-ferroelectric combinations for which the graphs in figures were obtained are:

a) on the effective permittivity variation graphs $\varepsilon_{eff}(y, \boldsymbol{E})$:

– $(1–y)$ $Ba_2Zn_{1.2}Cu_{0.8}Fe_{12}O_{22}$ / y $Ba_xSr_{1-x}TiO_3$ (y = 0.3 ÷ 0.9; with x like parameter) – continuous curves, respectively $(1-y)$ $Ba_{0.8}Sr_{0.2}Fe_{12}O_{19}$ / y $Ba_xSr_{1-x}TiO_3$ (y = 0.5 ÷ 0.9; with x = 1 – minimal curves) – dotted curves. A slight variation of the ferroelectric phase permittivity occurs when x varies (x = 0.75–1), consequently the curves are proximate if ***E*** and y are constant. When the applied electric field increases, the concentration of the electric phase necessary to obtain higher values of ε_{eff} is lower (curves are rising faster for higher ***E***). Polarizing field orientates the dipoles, but fields higher than about 20 kV/cm can affect the equilibrium forces inside the material phase.

b) on the effective permeability variation graphs $\mu_{eff}(1–y, \boldsymbol{H})$:

– $(1–y)$ $Ba_2Zn_{2-c}Cu_cFe_{12}O_{22}$ / y $Ba_{0.9}Sr_{0.1}TiO_3$ (y = 0.3÷ 0.9; with c like parameter) – continuous curves, respectively $(1-y)$ $Ba_{0.8}Sr_{0.2}Co_{2d}$ $Fe_{(12-2d\ )}O_{19}$ / y $Ba_{0.9}Sr_{0.1}TiO_3$ (y = 0.5 ÷ 0.9; with d = 0.9) – dotted curves. Ferrite phase permeability is greater for the composite with M hexaferrite, the permeability variation being lower with substitution degree modification inside the magnetic phase (for the composite with Y hexaferrite). Consequently, the composite permeability evolves similarly, the applied magnetic field determining a bit more abrupt variation of the effective permeability for higher ***H*** and for higher magnetic phase concentrations. Fields higher than 10–12 kOe will be not applied for this kind of nanocomposites, the magnetic moments risking becoming insensible to alternate fields.

In conclusion, the effective permittivity / permeability plots are shifting to higher values when the polarizing fields are increasing, but fields higher than a superior limit of a specific domain for each material are not recommended. The effect is nonlinear and our simulation method offers us the possibility to correlate the structure details with the applied field intensity and to understand the induced modifications.

5. DISCUSSIONS AND CONCLUSIONS

The existing theories to predict the effective electromagnetic parameters of the multi-components composites are based on: the mixture law, the Maxwell-Garnett equations or the Bruggeman effective medium theory (EMT). Each of them have strong limitations and represent more or less fair approximations of the real

cases of composite materials used in practice. The mixture law is useful in some cases where each component has a clearly definite and preponderant contribution to an effective parameter of the composite. The ferrite-ferroelectric nanocomposites can be included in such of cases, the composites presenting a magnetic, respectively electric constitutive phase.

According to the composite material structure, the mixture law has different forms, such as parallel connection model and series connection model. For the composite material with powder mixture, the mixture law can be written as the relation (9) [1], with particular forms (10) and (11). An improved form for the mixture law was proposed in this paper, which to describe with a high fidelity the mixture effective permittivity/permeability (12), (13), having coefficients depending on the control parameters of the structure (substitution degree in the compound constituents, substitution ions properties, ferrite internal order, polarizing fields).

Coefficient dependence on the substitution degree in the compound constituents is function of the physical properties of the substitutive ions and their concentration. The effective permittivity of the nanocomposite suffers slight modification by substitution of the Ba ions with Sr in the barium perovskite lattice, the coefficient which represent the exponent of $\left(\ln \varepsilon_b\right)$ in the derived mixture law varying the most. The ct_b' coefficient variation describes the electric moment modification of the substituted perovskite lattice. For the composite with *M*, respectively *Y* hexaferrites the permittivity coefficients evolution is similar, their report ensuring the lower values of effective permittivity for the *M* composite with lower polarizability.

Coefficient dependence on the substitution in hexaferrite with ions with different size and magnetic moment illustrate the modulation of the effective permeability by substitution methods. The substitution ions are modifying the spin equilibrium configuration of the hexaferrite and consequently the magnetic behavior of the nanocomposite. A increasing of the μ_{eff} with a few percents can be obtained by substituting in the hexaferrite the Ba and Zn ions without magnetic moment with ions presenting non-zero magnetic moment, like Cu, Co or Mn. The iron substitution in the hexaferrite lattice induces either an effective permittivity decreasing, when this is an wanted effect, but the chemical stability of ferrite the can be affected.

Coefficient dependence on the polarizing fields indicate us a shifting of the effective permittivity / permeability plots to higher values, more accentuate when the concentration of the ferroelectric / magnetic phase increases, if the polarizing fields are increasing up to a limit. The superior limit is specific to each material and can be found by our simulation methods as the polarizing field values for which the

secondary effects appears. The nonlinear character of this variation is imposed by the polarization modification induced to the samples, limited by the equilibrium of the structural forces.

The obtained results are punctually confirmed by literature ([2, 9, 19, 20] and so on). Not a continuous variation of the quantities computed here is available in the different author papers, especially concerning the polarizing field induced modifications, but a medium relative error was possible to be estimated for our results, of less or equal than 4 %, for the whole considered domain of working frequencies (20 to 40 GHz).

The results are also affected by the fact that the composed material permittivity and permeability present frequency dispersion [1]. A complete study of this phenomena was made in the case of the $(1–y)$ $Ba_{0.8}Sr_{0.2}Fe_{12}O_{19}$ / y $Ba_{0.9}Sr_{0.1}TiO_3$, $y = 0.5 \div 0.9$ composite and our conclusion was that an additional error of less than equal 1.5 % can be introduced by ignoring this effect, more important in the first quarter of the considered frequency range which is closer to a nanocomposite structural resonances.

The frequency dispersion of the electromagnetic parameters of the nanocomposite can be important in different applications where the wide band devices works and can affect the invariability of the transfer function over the whole frequency band. This study will make the subject of our future work. The frequency domain where our analysis was performed was chosen considering the working frequencies of the hexaferrite-ferroelectric composite applications developed until now [21, 22, 23] and is above the strong dielectric resonance peak observed above 0.1–6 GHz for this kind of nanocomposites.

A ferrite-ferroelectric nanocomposite domain of tunability can be reported on the basis of our study, ranging from 7 to 36%, depending upon each particular structure details. The considered control factors were mainly the concentration of phases, the substitution in the compound constituents and the polarizing fields, which can action like mono-factors or combined in pairs (concentration associated with substitution ion properties; concentration associated with polarizing field, etc.) for higher and refined induced modifications.

Acknowledgements. This paper was supported by the project PERFORM-ERA "Postdoctoral Performance for Integration in the European Research Area" (ID-57649), financed by the European Social Fund and the Romanian Government.

REFERENCES

1. Y. Bai, *The Ferroelectric-Ferromagnetic Composite Ceramics with High Permittivity and High Permeability, in Hyper-Frequency, Ferroelectrics*, edited by Indrani Coondoo, InTech, 2010, p. 187.

K. Satou, H. Ikezoe, S. Mitsuoka, K. Nishio and S. C. Jeong, Phys. Rev. **C 65**, 054602 (2002).

2. E. Selezneva, *Magnetoelectric Composites Based on Hexagonal Ferrites*, PhD Thesis, Universidade de Aveiro 2008.
3. D. V. Karpinsky, E. K. Selezneva, I. Bdikin, F. Figueiras, K. E. Kamentsev, Y. Fetisov, R. C. Pullar, J. Krebbs, N. M. Alford, A. L. Kholkin, *Development of Novel Multiferroic Composites Based on $BaTiO_3$ and Hexagonal Ferrites*, in Proceedings of the Symposium I – Engineered Multiferroics-Magnetoelectric Interactions, Sensors and Devices, **1161**, p. 101 (2009).
4. A. Bahadoor, Y. Wang, M. N. Afsar, *Complex permittivity and permeability of barium and strontium ferrite powders in X, KU, and K-band frequency ranges*, J. Appl. Phys., **97**, 10F105 (2005).
5. U. Adem, *Preparation of $Ba_xSr_{1-x}TiO_3$ Thin Films by Chemical Solution Deposition and their Electrical Characterization*, PhD thesis, The Graduate School of Natural and Applied Sciences of the Middle East Technical University, Ankara, Turkey, 2003.
6. A. Vorobiev, S. Gevorgian, M. Löffler, E. Olsson, at The International Symposium on *Integrated Functionalities* (ISIF 2011), Cambridge, England, July 31-August 4, 2011, Poster No. 153357.
7. D. Ionescu, I. B. Ciobanu, *HF Study of the Electrical Permittivity for Some Perovskite-Like Systems from the Two Dimensional Perovskite Layer Family*, Romanian Journal of Physics, **54**, *9–10*, 899 (2009).
8. D. Ionescu, I. Bogdan, *Simulation Determination of the Tunable Electromagnetic Parameters for the Sc Doped BaM Metaferrites in GHz Range*, Romanian Reports in Physics, **64**, *2*, 411 (2012).
9. S. S. Kalarickal, D. Ménard, J. Das, C. E. Patton, X. Zhang, L. C. Sengupta, S. Sengupta, *Static and high frequency magnetic and dielectric properties of ferrite-ferroelectric composite materials*, J. Appl. Phys., **100**, 084905 (2006).
10. M Liu, O Obi, J Lou, S Stoute, Z Cai, K Ziemer, N X Sun, *Strong magnetoelectric coupling in ferrite/ferroelectric multiferroic heterostructures derived by low temperature spin-spray deposition*, J. Phys. D: Appl. Phys., **42**, 045007 (2009).
11. M. B. Shelar, R. N. Jadhav, V. Puri, *Microwave Studies of Ferrite-Ferroelectric Composites Preparred Through Self Propagating Auto Combustion Route*, Progress in Electromagnetics Research C, **17**, 55 (2010).
12. L. C. Sengupta, S. Sengupta, *Ceramic Ferrite/Ferroelectric Composite Material*, Pat. No. 6063719 (2000).
13. S Cojocaru, *Effect of boundary conditions on magnetization of a nano-size ferromagnet*, Romanian Reports in Physics, **64** (Supplement), 1207–1211 (2012).
14. J. van Landuyt, S. Amelinckx, *Multiple Beam Direct Lattice Imaging of the Hexagonal Ferrites*, Journal of Solid State Chemistry, **9**, 103 (1974).
15. Y. Bai, F. Xu, L. Qiao, J. Zhou, L. Li, *The Static and Hyper-Frequency Magnetic Properties of a Ferromagnetic-Ferroelectric Composite*, Journal of Magnetism and Magnetic Materials, **321**, *3*, 148 (2009).
16. E. Burzo, *Magnetic properties and exchange interactions in rare-earth-iron-based compounds*, Romanian Reports in Physics, **63** (Supplement), 1316–1328 (2011).
17. J. W. Wang, A. L. Geiler, V. G. Harris, C. Vittoria, *Numerical simulation of wave propagation in Y and Z-type hexaferrites for high frequency applications*, Journal of Applied Physics, **107**, 09A515 (2010).
18. H. Zhang, L. Li, J. Zhou, J. Bao, Z. Yue, Z. Gui, *Microstructure and properties of Co_2Z hexaferrite prepared by gel self-propagating method*, Journal of Materials Science: Materials in Electronics, **11**, *8*, 619 (2000).
19. J. L. Capitaneo, V. da R. Caffarena, T. Ogasawara, M. S. Pinho, *Performance of Radar Absorbing Nanocomposites by Waveguide Measurements*, Materials Research, **11**, *3*, 319 (2008).

20. N. Rezlescu, E. Rezlescu, F. Tudorache, P.D. Popa, *Gas sensing properties of porous Cu-, Cd- and Zn- ferrites*, Romanian Reports in Physics, **61**, *2*, 223–234 (2009).
21. S. Sengupta, D. Menard, R. Cox, S. Kalarickal, *Ferrite-Ferroelectric Composite Materials for Microwave and Millimeter Wave Device Applications*, Final Progress Report, Aro Grant No.: DAAD19-99-1-0170 (2000).
22. V. G. Harris, A. Geiler, Y. Chen, S. D. Yoon, M. Wu, A. Yang, Z. Chen, P. He, P. V. Parimi, X. Zuo, C. E. Patton, M. Abe, O. Acher, C. Vittoria, *Recent advances in processing and applications of microwave ferrites*, Journal of Magnetism and Magnetic Materials, **321**, 2035 (2009).
23. R. V. Petrov, A. S. Tatarenko, G. Srinivasan, J. V. Mantese, *Antenna miniaturization with ferrite ferroelectric composites*, Microwave and Optical Technology Letters, **50**, *12*, 3154 (2009).